Progress In Electromagnetics Research C, Vol. 91, 97–113, 2019

Design of Miniaturized Quad-Band Dual-Arm Spiral Patch Antenna for RFID, WLAN and WiMAX Applications

Ayia A. S. A. Jabar and Dhirgham K. Naji*

Abstract—In this paper, a new design approach is presented for achieving a miniaturized quad-band microstrip patch antenna (MPA) suitable to be used for 915-MHz (UHF band), 2.45- and 5.8-GHz (ISM band), and 3.5-GHz (WiMAX band). The proposed antenna is called modified square spiral antenna (MSSA) which is composed of a modified dual-arm square spiral patch strip structure and a tapered-ground plane with coplanar wave-guide (CPW)-fed configuration to feed this antenna, all printed on the top side of an FR4 substrate. The proposed antenna is designed through intermediate systematic design steps of antennas starting from a conventional strip-fed rectangular MPA and ending by achieving MSSA. A CST Microwave Studio (CST MWS) is used to model the designed antenna, and simulation results, in terms of return loss (S_{11}), realized peak gain and efficiency, besides radiation patterns, are obtained. To validate the design concept, the antenna structure is fabricated, and the simulated and measured S_{11} results nearly coincide with each other. The proposed antenna is characterized by miniaturized size of $28 \times 28\,\text{mm}^2$, and based on measured -10-dB S_{11} result, MSSA has four bands, band 1: 915 MHz (872–929 MHz), band 2: 2.45-GHz (2395–2510 MHz), band 3: 3.5-GHz (3470–3550 MHz), and band 4: 5.8-GHz (5698–5900 MHz).

1. INTRODUCTION

It is well known that one of the important electrical devices, which receives and/or transmits information through space is antenna. Recently, there has been increasing interest for multiband, omnidirectional antennas characterized by miniaturized size and simple realization to meet the requirements needed by modern standard wireless communication systems. These communication standards are accessed daily by people over the world, such as Radio Frequency Identifications (RFID), Wireless Local Area Network (WLAN), Bluetooth-enabled devices, satellite communications, the fifth-generation (5G) cellular networks, and Worldwide Interoperability for Microwave Access (WiMAX). [1]. Thus, multiband antenna should cover the desired bands allocated for these standards, 915 MHz (860–960 MHz), 2.45 GHz (2.4–2.5 GHz), 5.8 GHz (5.725–5.875 GHz) for RFID and WLAN bands, 3.5 GHz (3.4–3.6 GHz) for 5G and WiMAX band, etc.

Three main types of multiband printed antennas that have been reported in the recent few years to satisfy the aforementioned bands with compact size are monopole antennas (MAs), slot antennas (SAs), and patch antennas (PAs) [2–11]. The conventional technique for realizing multiband characteristics to these antennas is either by addition of multi-radiating elements to the patch of MS [2–5] and PA [6–8] or inserting slots or notches in the radiating element of SA [9–11]. The idea behind this technique is getting different current paths at the surface of these antennas that lead to resonating at various frequencies.

Received 17 January 2019, Accepted 1 March 2019, Scheduled 21 March 2019
* Corresponding author: Dhirgham Kamal Naji (dknaji73@yahoo.com).
The authors are with the Department of Electronic and Communications Engineering, College of Engineering, Al-Nahrain University, Baghdad, Iraq.

It is known that the dominant resonant frequency for most of the antennas is so far dependent on the physical dimension of their radiating elements and subsequently limits the antenna miniaturization to a certain extent. Hence, the design of miniaturized multiband antennas is highly attractive, and persistent attempts for new solutions and approaches are presented by researchers, in particular for antennas operating at lower frequency bands [12–17]. In [12], a slotted triangular MA was presented to cover dual bands used for RFID systems and operated in the frequency ranges of (0.797–1.004 GHz) and (2.234–2.934 GHz). A compact coplanar waveguide (CPW)-fed folded SA with overall dimensions of $30\times30\,\text{mm}^2$ was proposed in [13] to operate at four bands for 0.94/2.45/5.8-GHz RFID and 2.45/3.5/5.5-GHz WiMAX/WLAN applications. In this design, to achieve multiband operation with miniaturize size, three slots and four L-shaped and two U- and F-shaped branches were used as additional resonators. In [14], a printed planar spiral-shaped folded strip MA was proposed for resonating at different frequency bands between 0.5 and 5.6 GHz suitable for low frequency biomedical band besides other wireless bands such as Bluetooth, WLAN, ZigBee, and LTE bands. CPW-fed technique was used to excite this antenna, and the width of spiral strip was controlled to vary within the restricted size $23\times40\,\text{mm}^2$ of the optimized antenna for getting the desired bands. The antenna presented in [15] was optimized to operate effectively in ISM bands (2.4 and 5.8 GHz), as well in 5G bans (0.7 and 3.5 GHz). A CPW was used for feeding this antenna which comprises one circular disc and two circular rings, and its overall dimensions are 175 mm × 105 mm. A multiband Koch fractal PA is proposed in [16] for operating at triple frequency bands, 915 MHz, 2.45 GHz, and 5.8 GHz. A miniaturized metamaterial based MA was designed in [17] to operate at cellular standards such as GSM 900 (0.9 GHz), Wi-Fi (2.5 GHz), and WiMAX (3.5 GHz). To shift the resonance frequency for the lower band to 0.9 GHz, an additional layer (copper) was connected via shorting pin to the antenna radiating layer resulting in reduction in electrical size about 76% of the proposed design. Although most of the aforementioned designed antennas have achieved multiband characteristics, they are either large in size or complex in geometrical structure.

In this paper, a new design approach is presented for achieving a miniaturized quad-band microstrip patch antenna (MPA) suitable for 0.915/2.45/5.8-GHz RFID tag and 2.45/3.5-GHz WiMAX/WLAN applications. The proposed antenna is called modified square spiral antenna (MSSA) and has a size of $28\times28\,\text{mm}^2$. A CST Microwave Studio (CST MWS) is used to model the designed antenna. A simulation result in terms of return loss (S_{11}) is compared with the measured result, and a good agreement between them has been obtained. Then the simulation results for the proposed antenna, including return loss, surface current distribution, gain, and efficiency besides the radiation pattern at the specified resonance frequencies, are discussed.

2. GEOMETRY OF THE PROPOSED ANTENNA

The 3D simulation model and fabricated structure of the finalized proposed designed antenna, modified square spiral antenna (MSSA), is shown in Figure 1. The antenna is printed on the front side of an FR4 substrate ($L_{sub} \times W_{sub}$) of (28 mm × 28 mm) with thickness h_{sub} of 1.6 mm and relative permittivity $\epsilon_r = 4.3$. The FR4 substrate is available in the Lab, and it is used to fabricate the proposed antenna. The authors aware that there are low-cost substrates, such as Kappa 438 and ISOLA A380, and they may be used for better quality factor, improving antenna input return loss (selectivity). However, these materials are not available in our fabrication lab. The patch of antenna, length ($L_p = 11.5\,\text{mm}$)× width ($W_p = 24.5\,\text{mm}$) is inscribed with a modified dual-arm spiral strip configuration connected to the coplanar waveguide (CPW) structure via a strip of length L_1 and width t_2. The vertical (horizontal) spiral's width is $t_1(t_2)$ whereas the spacing between them is $t_2(t_1)$. The tapered ground plane has length L_g, and the length (width) of CPW is represented by symbols L_f ($W_f = 2\,\text{mm}$) for feeding antenna through a sub-miniature-A (SMA) connector. Table 1 lists the optimized values of antenna parameters.

3. DESIGN PROCEDURE

The proposed designed MSSA, characterized by miniaturized size and multiband behavior, is achieved by using a procedure which comprises five design steps. Figure 2 displays the evolution process for designing the five antennas (Ant0–Ant4), all having the same size of (28 mm × 28 mm). Figures 2(a)–(d) show the designed antennas that lead to the proposed antenna, MSSA, as shown in Figure 2(e).

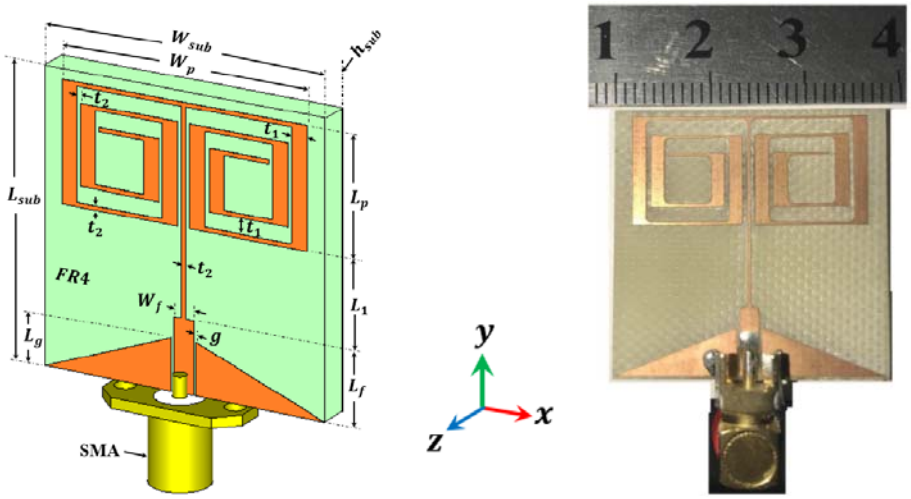

Figure 1. Configuration of the proposed antenna, MSSA. (a) 3D simulation model. (b) Fabricated structure.

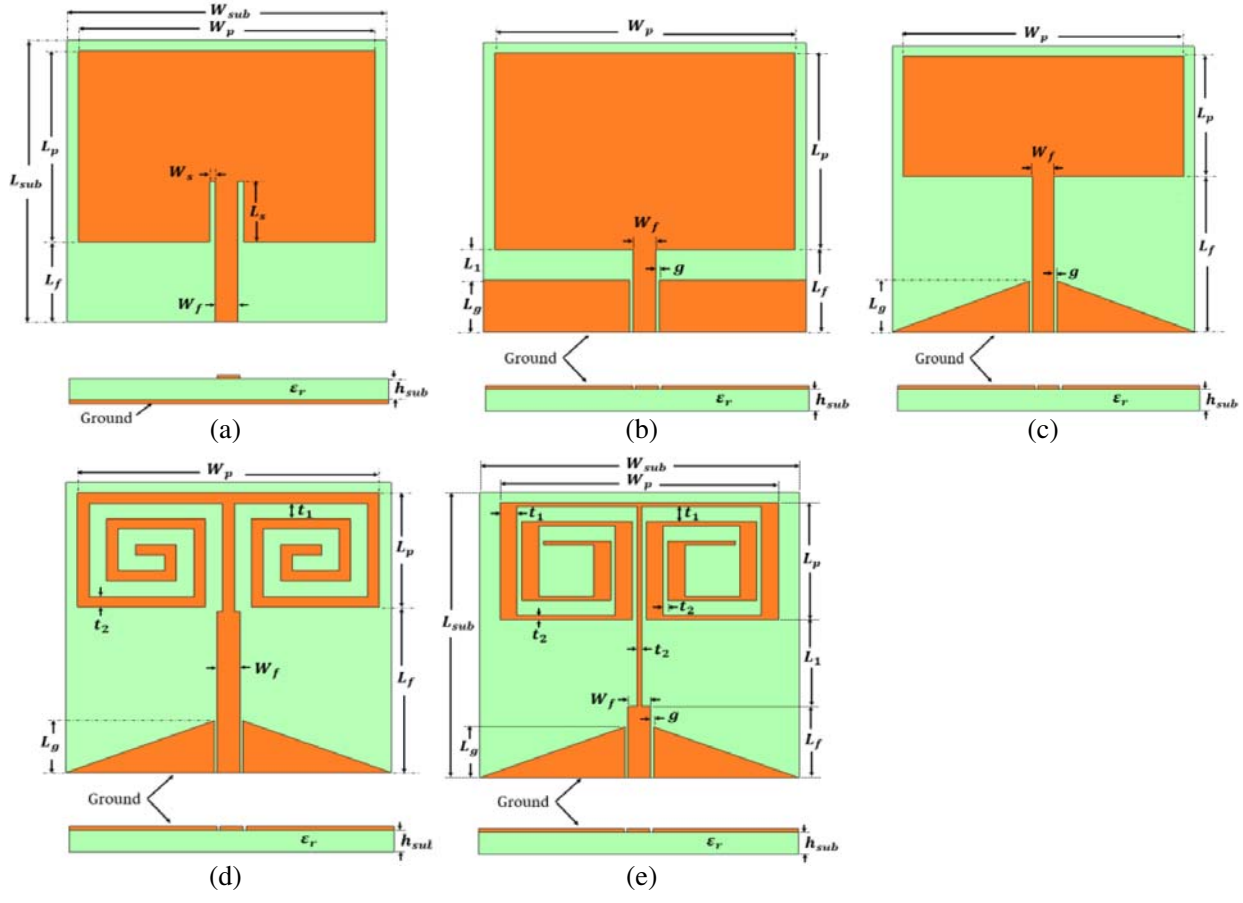

Figure 2. The evolution design procedure for the proposed antenna, MSSA. (a) The ordinary stripline-fed MPA (Ant0). The CPW-fed (b) ordinary MPA (Ant1), (c) MPA with tapered ground plane (Ant2), (d) ordinary square spiral MPA (Ant3) and (e) modified square spiral MPA (Ant4).

The first designed antenna, as shown in Figure 2(a), is a conventional strip-fed MPA (Ant0) designed by applying equations of the transmission line model to resonate at 3.5-GHz WiMAX band. Then intermediately designed CPW-fed MPAs are obtained during the design procedure until achieving MSSA (Ant4) that has the desired operating frequency bands. Table 1 shows the parameter values of the designed antennas (Ant0–Abt4) while Figure 3 shows their CST simulated return loss (S_{11}) results. The next sections describe and investigate in detail the design procedure for these antennas as well their simulation S_{11} results.

Table 1. The final dimensions of the designed antennas.

Parameter	Value (mm)				
	Ant0	**Ant1**	**Ant2**	**Ant3**	**Ant4**
$\mathbf{L_{sub}}$	28.0	28.0	28.0	28.0	28.0
$\mathbf{W_{sub}}$	28.0	28.0	28.0	28.0	28.0
$\mathbf{h_{sub}}$	1.5	1.5	1.5	1.5	1.5
$\mathbf{L_p}$	19.0	19.0	12.0	12.0	11.5
$\mathbf{W_p}$	26.0	26.0	26.0	26.0	24.5
$\mathbf{L_f}$	8.0	8.0	15.0	15.0	7.0
$\mathbf{W_f}$	2.0	2.0	2.0	2.0	2.0
$\mathbf{L_s}$	4.0	-	-	-	-
$\mathbf{W_s}$	0.4	-	-	-	-
$\mathbf{g}$	-	-	0.25	0.25	0.25
$\mathbf{L_g}$	-	6.0	6.0	5.0	5.0
$\mathbf{L_1}$	-	2.0	9.0	9.0	8.5
$\mathbf{t_1}$	-	-	-	1.5	1.5
$\mathbf{t_2}$	-	-	-	1.0	0.4

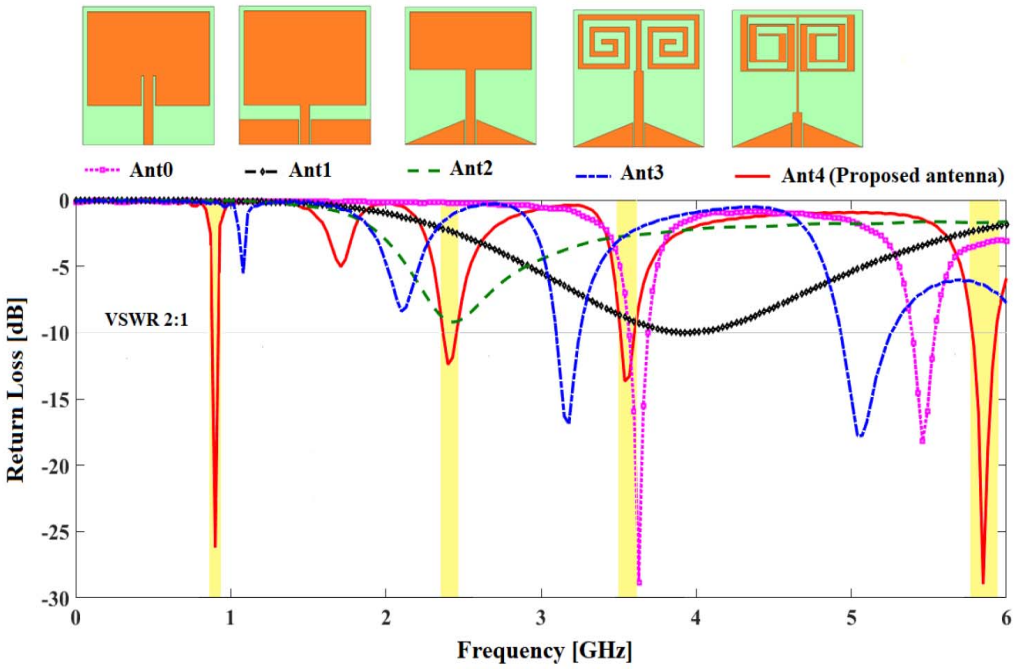

Figure 3. Simulated return loss for the five designed antennas.

3.1. Design of the Conventional MPA

As stated in the previous section, for achieving the antenna having both miniaturized size and desired multiband operation for covering sub-6 GHz frequency bands, a conventional strip-fed rectangular MPA (Ant0) is considered as a good choice to begin with. To do that, transmission line equations, Eqs. (1)–(4), are used for designing the conventional strip-fed rectangular MPA [18]

$$\varepsilon_{eff} = \frac{\varepsilon_r + 1}{2} + \frac{\varepsilon_r - 1}{2}\left(\frac{1}{\sqrt{1 + 12h/W}}\right) \tag{1}$$

where ε_r, h, W are dielectric constant, height of the substrate, and width of the substrate, consecutively. The length and width of antenna identify antenna resonance. The width of antenna for dominant mode resonance is given as:

$$L = \frac{1}{2f_r\sqrt{\varepsilon}_{eff}\sqrt{\mu_0\varepsilon_0}} - 2\Delta L \tag{2}$$

where,

$$\Delta L = 0.412h\frac{(\varepsilon_{eff} + 0.300)}{(\varepsilon_{eff} - 0.258)}\frac{\left(\frac{W}{h} + 0.262\right)}{\left(\frac{W}{h} + 0.813\right)} \tag{3}$$

Here c is the speed of light in space, and f_r is the resonance frequency of antenna. The width of patch antenna is given by

$$W = \frac{c}{2f_r}\sqrt{\frac{2}{\varepsilon_r + 1}} \tag{4}$$

By applying these equations, the geometrical parameters, patch width ($W_p = 26.32\,\text{mm}$), and patch length ($L_p = 19.26\,\text{mm}$) of the conventional MPA have been calculated by assuming the resonant frequency $f_r = 3.5\,\text{GHz}$ (WiMAX band), and the relative permittivity is given as $\varepsilon_r = 4.3$ (FR4) while the height of the substrate is $h_{\text{sub}} = 1.5\,\text{mm}$. Then, an inset-fed MPA (length L_s and width W_s), as illustrated in Figure 4, is simulated by employing the full wave electromagnetic CST MWS with the calculated values of L_p and W_p described above as an initial length and width of the rectangular patch antenna connected to the $50\,\Omega$ SMA through the stripline of length L_f and width $W_f = 2\,\text{mm}$. After fine-tuning the antennas' geometrical parameters, the optimized values of these parameters are listed in Table 1. As shown in Figure 5, the simulated return loss of the conventional designed antenna operates at dual-frequency bands with resonance frequencies $f_{r1} = 3.6\,\text{GHz}$ and $f_{r2} = 5.4\,\text{GHz}$ with

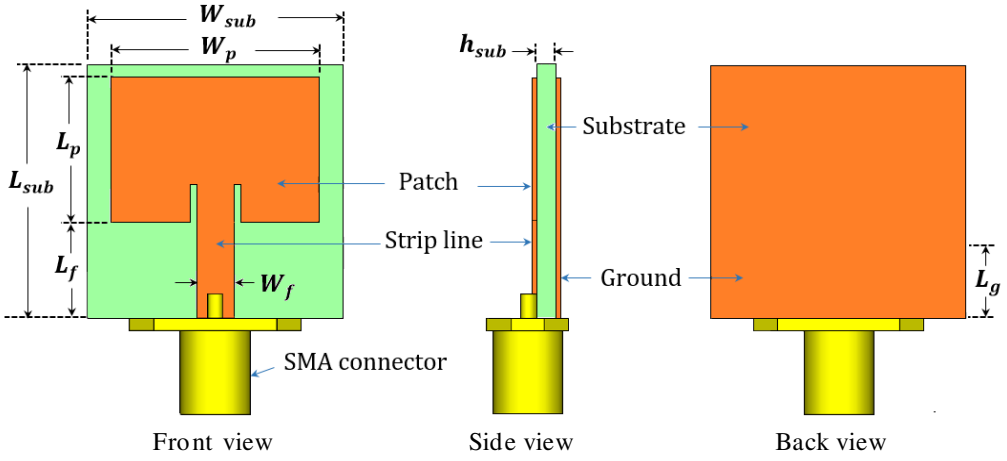

Figure 4. Conventional microstrip inset-fed MPA, Ant0.

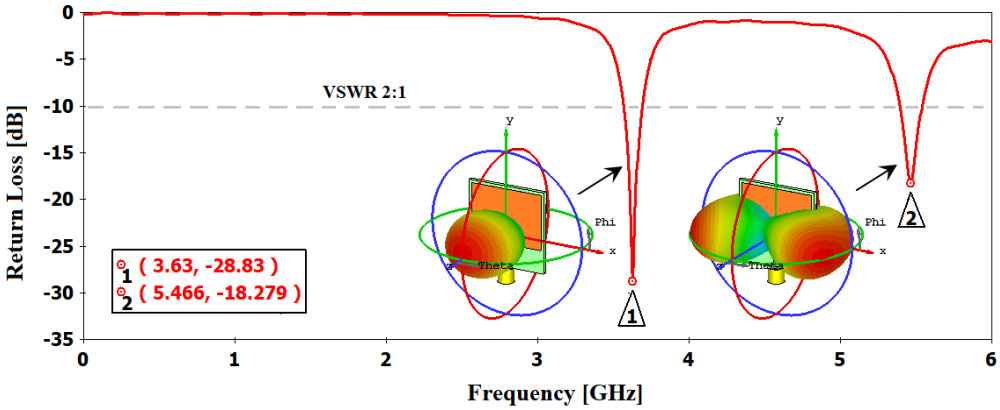

Figure 5. S_{11} plot and radiation pattern for the conventional inset-fed MPA.

-10-dB S_{11} bandwidth of 200 MHz for the first band (3.5 GHz–3.7 GHz) and 170 MHz for the second band (5.37 GHz–5.54 GHz). The total radiation is in the front direction of antenna in 3.6 GHz and in the right and left side directions of antenna in 5.4 GHz. This antenna has patch dimensions ($L_p \times W_p$) of (19 mm $\times$ 26 mm), and the total substrate dimensions ($L_{\text{sub}} \times W_{\text{sub}}$) are (28 mm $\times$ 28 mm).

3.2. Design of a Reference Antenna

The conventional MPA has been successively designed based on Eqs. (1)–(4) to operate at the desired resonance frequency $f_r = 3.5$ GHz. A reference antenna (RA) with tapered ground plane and fed by CPW technique is required to be resonated at $f_r \cong 2.45$ GHz (RFID and WLAN bands). To do that, initially, a previously microstrip-fed antenna is redesigned with the same geometrical parameters except using a partial ground of length L_g at the back side of the substrate, as shown in Figure 6(a). Later on, a microstrip antenna with strip feed is replaced by a counterpart CPW feed to produce the desired reference antenna (RA) or Ant1 as shown in Figure 6(b).

Figure 7 shows the return loss plot for applying both the CPW feed and microstrip feed to the designed antennas. It can be noticed that the strip-fed conventional MPA with ground (partial ground) has lower resonant frequency f_r of 3.63 GHz at $S_{11} = -28.83$ dB (3.95 GHz at $S_{11} = -6.59$ dB), whereas the CPW-fed reference antenna (RA) resonates at $f_r = 3.92$ GHz at S_{11} of -9.8 dB. After that CPW-fed RA is designed from the conventional strip-fed MPA to operate at 3.92 GHz, the RA is redesigned to resonate at $f_r = 2.45$ GHz.

3.3. Design of a CPW-Fed Tapered Ground MPA

Figure 8(a) shows the designed CPW-fed tapered ground plane (Ant2) which has the same geometrical parameters of its counterpart Ant1 except using L_p of 12 mm instead of 19 mm as in Ant1. The return loss performance of RA is plotted in Figure 8(b). It is seen from this figure that this antenna resonates at 2.44 GHz at $S_{11} = -9.2$ dB. This antenna is used in the preceding evolution design process for designing the proposed antenna.

3.4. Dual and Modified Dual-Arm Square Spiral Patch Antennas

Depending on the previous designed antenna, Ant3 is evolved from Ant2 by forming its patch as a spiral strip having width $t_1 = 1.0$ mm, and the spacing between the strips t_2 is 0.5 mm. This antenna is called square spiral antenna (SSA) and shown in Figure 9(a).

The spiral turns increase the effective inductance and capacitance thereby modifying the surface current distribution and input impedance at the same time and exhibiting quaternary band resonance with small matching. In order to overcome this limitation, modified square spiral antenna (MSSA) with ($t_1 = 1.5$ mm and $t_2 = 0.4$ mm) as shown in Figure 9(b) has been proposed. This antenna resonates at

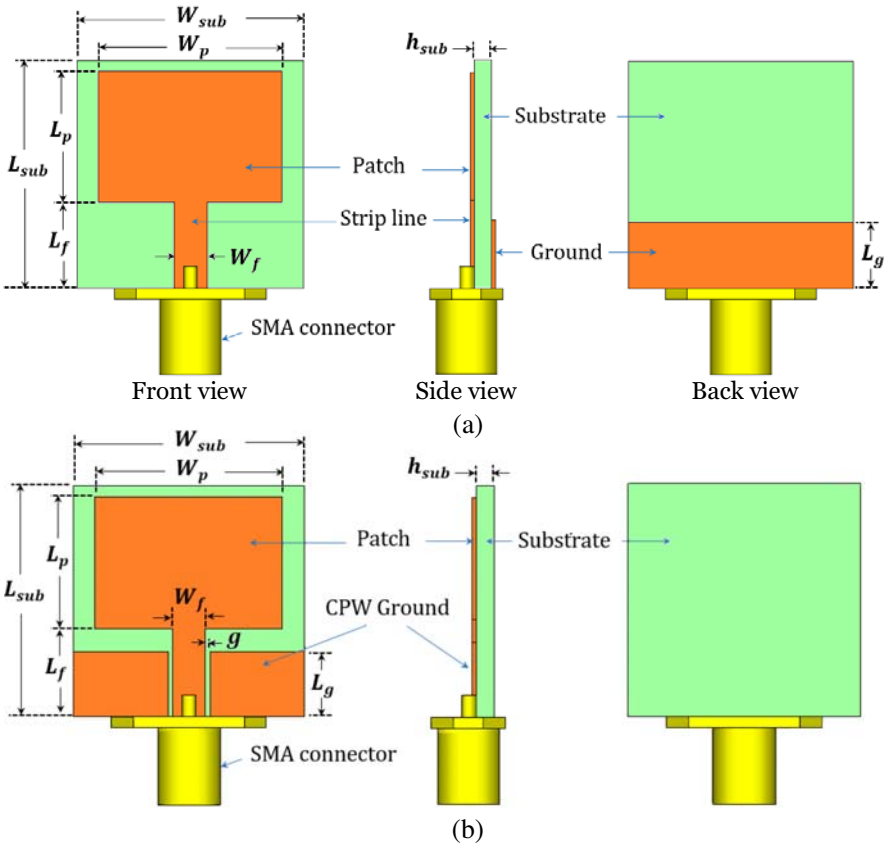

Figure 6. (a) Microstrip-fed MPA with partial ground. (b) CPW-fed MPA, the reference antenna (RA), Ant1.

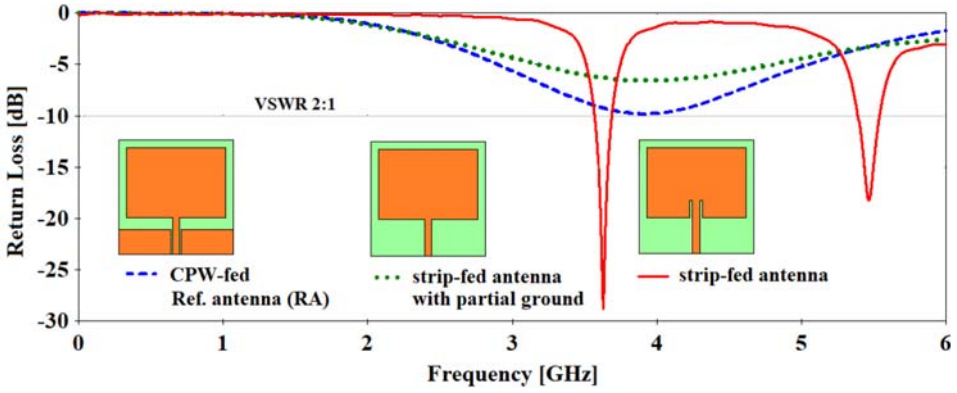

Figure 7. CST simulated return loss curves of various antennas.

four frequencies (i.e., 0.90 GHz, 2.41 GHz, 3.54 GHz, and 5.85 GHz) with matching less than −10 dB as shown in Figure 10. The return loss of the designed antennas is plotted in Figure 10, and the summarized results for the five designed antennas in terms of the jth lower, higher, and resonance frequency f_{Lj}, f_{Hj}, and f_{rj}, respectively, are illustrated in Table 2.

3.5. The Operating Concept of Quad-Band Antenna

To explore the dependent frequency bands on the number of spiral turns for the proposed antenna, the antenna is simulated for one-, two-, and three-turn spiral antennas, SPA1, SPA2, and SPA3, respectively.

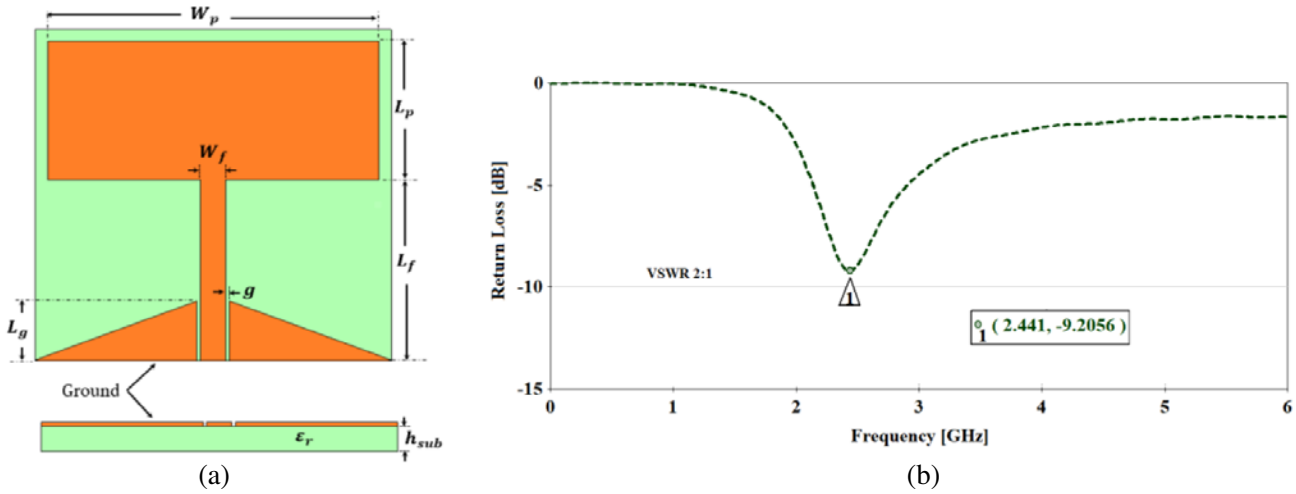

Figure 8. The CPW-fed MPA with tapered ground plane (Ant2) (a) and its plot of return loss against frequency (b).

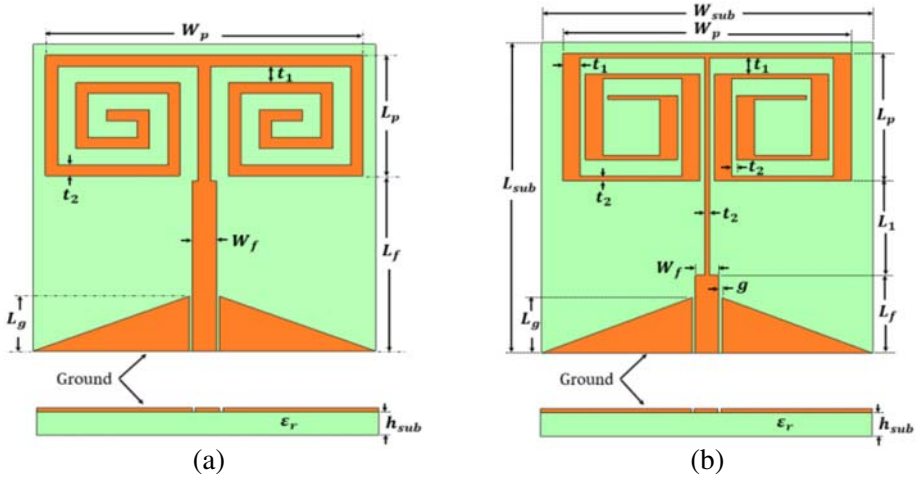

Figure 9. (a) The ordinary dual-arm square spiral antenna (SSA), Ant3. (b) The modified square spiral antenna (MSS), Ant4.

Table 2. The simulated and measured frequency bands of optimized antenna. Unit in [MHz].

Band number j	Simulation result			Measurement result		
	f_{Lj}	f_{Hj}	f_{rj}	f_{Lj}	f_{Hj}	f_{rj}
1	890	935	910	872	929	900
2	2368	2455	2410	2394	2510	2460
3	3510	3600	3550	3474	3547	3510
4	5780	5930	5850	5697	5903	5790

Figures 11(a)–(c) depict these three design steps as evolution process to attain SPA3 as the proposed antenna. Figure 12 shows the simulated return loss results for these antennas. It is seen from this figure that -10-dB S_{11} return loss of SPA3 covers four different frequency bands whereas both antennas SPA1 and SPA2 operate only throughout single band. Additionally, one can conclude from Figure 12 that SPA3 has the desired frequency bands with compact size.

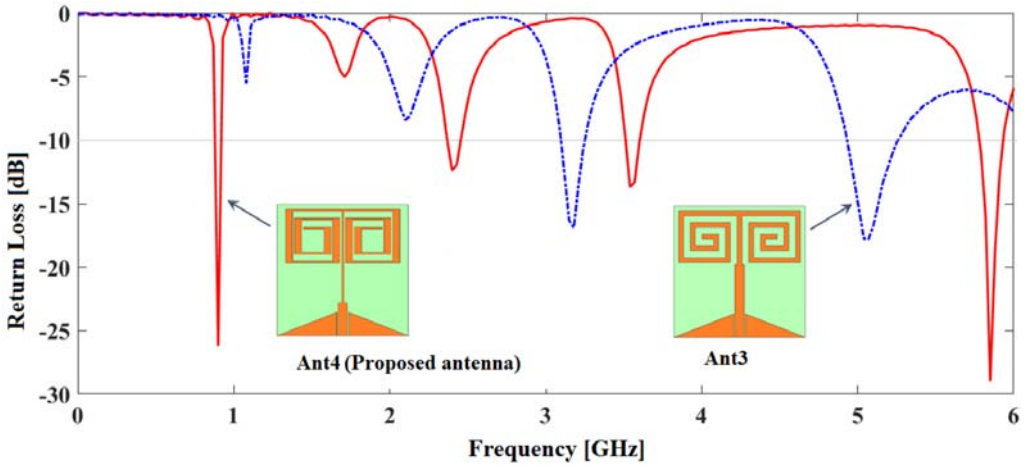

Figure 10. Simulated return loss for Ant3 and Ant4 (proposed antenna).

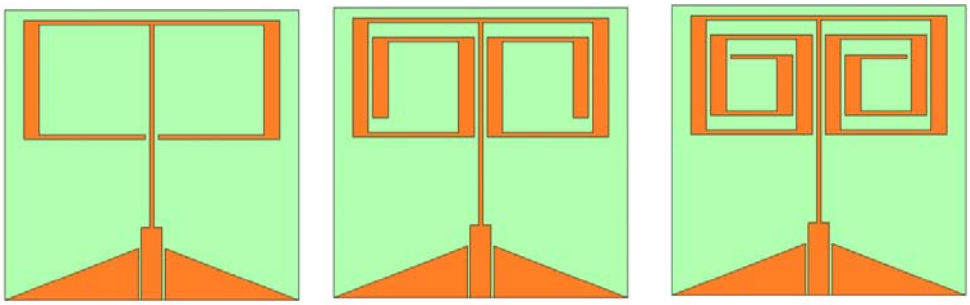

Figure 11. The proposed modified dual-arm spiral patch antenna (SPA). (a) One-turn spiral (SPA1). (c) Two-turn spiral (SPA2). (d) Three-turn spiral (SPA3) as proposed antenna.

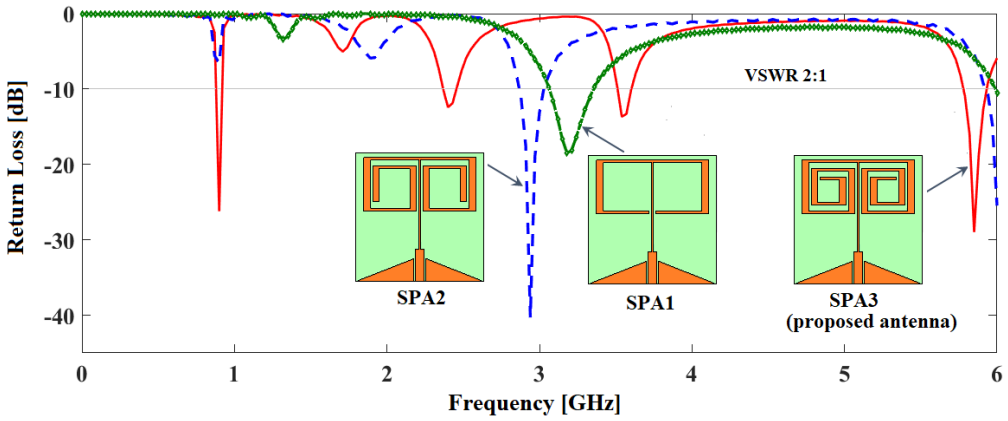

Figure 12. Simulated return loss plots for the proposed antennas shown in Figure 11.

The simulation results of the proposed antenna reveal that the real parts of input impedances of the antenna are 58, 60, 36, and 55 Ω at 0.9, 2.4, 3.55, and 5.85 GHz, respectively. These results clearly indicate that the antenna input impedance is nearly matched to 50 Ω of the feed line at the four operating frequencies.

3.6. Experimental Result and Discussion

To validate the CST simulated results obtained from CST MWS, the proposed antenna is fabricated, and its return loss is measured by using Agilent/HP N9923A 6 GHz Handheld RF Vector Network Analyzer in Figure 13. The simulated and measured return losses are plotted in Figure 14. It is clear from Figure 14 that simulated and measured results nearly coincide with each other over the four operating frequency bands. A slight difference between these results is due to the uncertainty in permittivity and height of the substrate or due to the fabrication misalignment. Also, it is demonstrated from the measured −10-dB S_{11} result that the proposed antenna has four bands: band 1, 915 MHz (872–929 MHz), band 2, 2.45-GHz (2395–2510 MHz), band 3, 3.5-GHz (3470–3550 MHz), and band 4, 5.8-GHz (5698–5900 MHz) which are suitable for RFID, WLAN, and WiMAX applications.

Figure 13. Photograph of Agilent/HP N9923A 6 GHz Handheld RF Vector Network Analyzer that employed for measuring return loss of the proposed antenna.

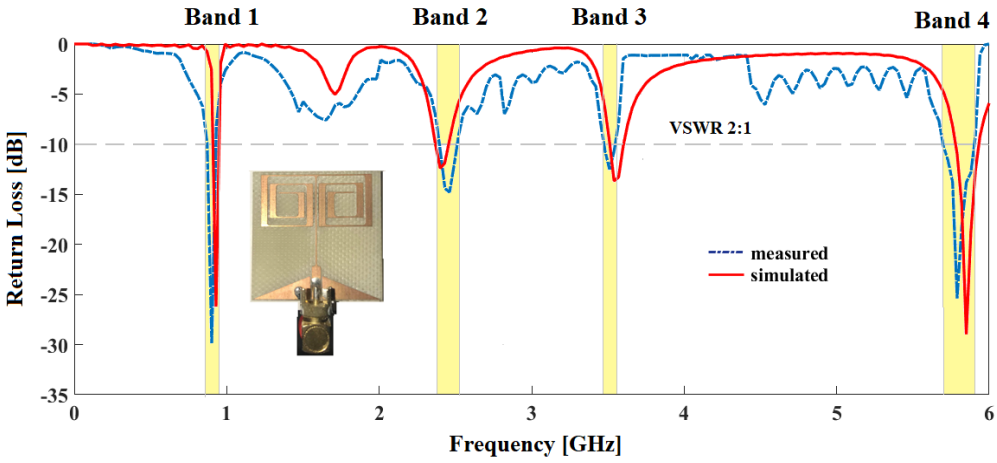

Figure 14. The simulated and measured return loss for the proposed antenna.

3.7. Characterization of the Proposed Antenna

This section presents the performance parameters of the proposed antenna in terms of surface current distribution and far-field features, gain, efficiency, and radiation patterns. Commercial software CST MWS is used to obtain these performance parameters.

3.7.1. Surface Current Distribution

The concept of multiband operation by introducing spiral strip as a radiator element for the proposed antenna can be clearly identified by investigating the current distribution at the resonance frequency in each operating band, bands 1–4. This is illustrated in Figure 15 by plotting the surface current density at 900 MHz (band 1), 2.4 GHz (band 2), 3.5 GHz (band 3), and 5.8 GHz (band 4). It is noticed from Figure 15(a) that at low operating frequency (large wavelength), more current flows at perimeter of the inner and outer spiral strips. In contrast, Figure 15(d) shows that the current distribution is reduced to flow in the outer spiral strip for higher frequencies (low wavelengths), and it is more concentrated along the CPW feeding line, inner strips, and at edges of the ground plane. This behavior of surface current distribution agrees well with the basic concept of antenna theory, and as a result the antenna is expected to be more efficient in terms of far-field radiation characteristic, gain, and efficiency when operating at higher frequencies. This fact will be proved in the next section.

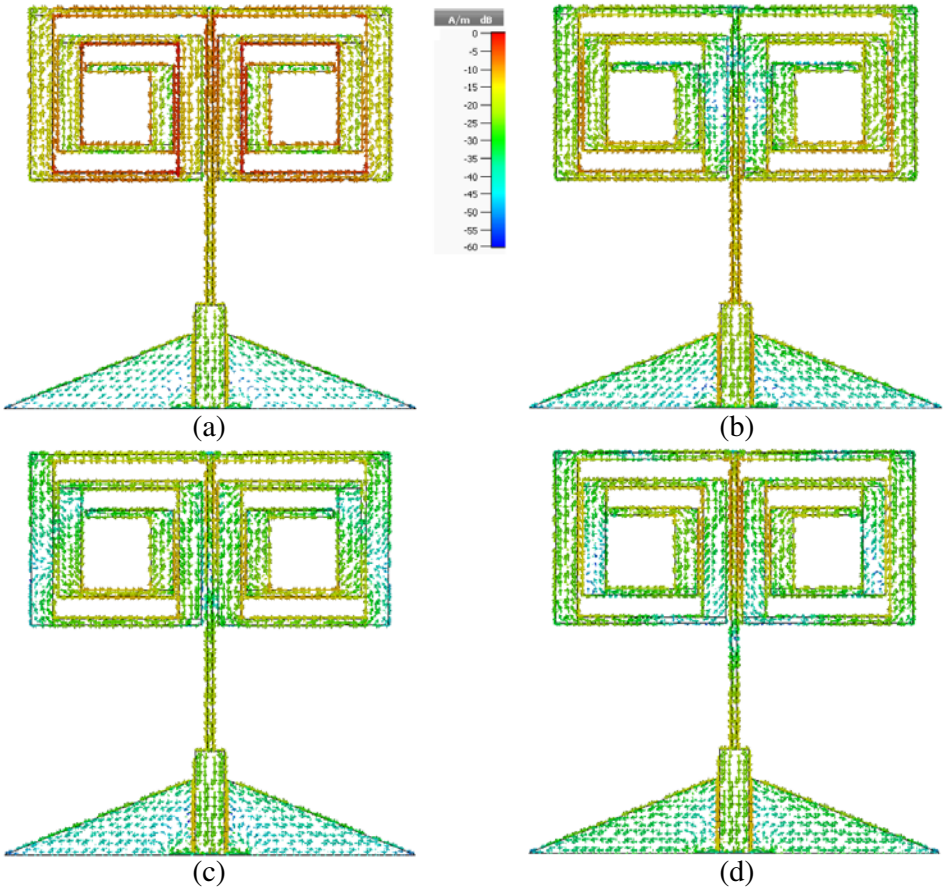

Figure 15. Simulated current distribution for the proposed antenna at four resonance frequencies. (a) 0.9 GHz. (b) 2.4 GHz. (c) 3.5 GHz. (d) 5.8 GHz.

It is well known that the effective electrical current path L_e of a dual-arm spiral antenna is related to its resonance frequency f_r, as the conventional dipole antenna, and it is approximately equal to half of the guided wavelength λ_g

$$\lambda_g = \frac{c}{f_r\sqrt{\varepsilon}_{eff}} \tag{5a}$$

$$\varepsilon_{eff} \cong \frac{\varepsilon_r + 1}{2} \tag{5b}$$

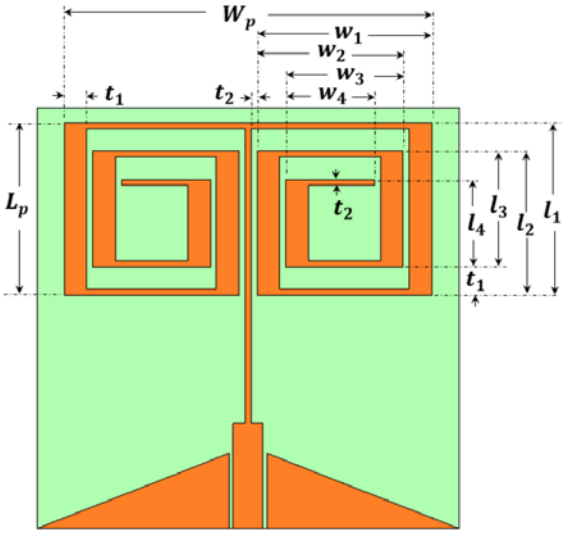

Figure 16. The proposed spiral antenna.

In the design of the proposed antenna, L_e for each f_r is set to the average value of spiral strip lengths, and current has flowed on their surfaces. As noticed from Figures 15 and 16, one can deduce that the effective current path $L_{0.9\,\mathrm{GHz}}$, $L_{2.4\,\mathrm{GHz}}$, $L_{3.55\,\mathrm{GHz}}$ and $L_{5.8\,\mathrm{GHz}}$ for 0.9, 2.4, 3.55, and 5.8 GHz, respectively, are given by

$$L_{0.9\,\mathrm{GHz}} = \frac{1}{2}\left[L_1 + L_p + \frac{W_p}{2} + \sum_{i=1}^{4}(l_i + w_i)\right] \tag{6a}$$

$$L_{2.4\,\mathrm{GHz}} = \frac{1}{2}\sum_{i=1}^{2}(l_i + w_i) \tag{6b}$$

$$L_{3.55\,\mathrm{GHz}} = W_p \tag{6c}$$

$$L_{5.8\,\mathrm{GHz}} = \frac{1}{2}(l_3 + w_3) \tag{6d}$$

where l_i and w_i are the ith length and width of the spiral strip structure, respectively, and their values depend on the patch length and width L_p and W_p, respectively, and the spiral strip thicknesses t_1 and t_2. Based on Figure 16, these two parameters are calculated as

$$l_i = L_p - (i-1)(t_1 + t_2) \tag{7a}$$

$$w_i = 0.5\left[W_p - (2i+1)\,t_2 - 2\,(i-1)\,t_1\right], \quad i = 1, \ldots, 4 \tag{7b}$$

The values of these geometric parameters are calculated and listed in Table 3. As a result, Eqs. (6a)–(6d) are calculated by substituting the aforementioned values listed in Table 3, and their corresponding guided wavelengths are found from Eqs. (7a) and (7b). Table 4 presents the effective current path L_e and the wavelength for each f_r, and it is clear from this table that they have nearly the same values.

Table 3. The geometric parameters of the spiral antenna.

Parameter	Value (mm)	Parameter	Value (mm)	Parameter	Value (mm)
L_p	11.5	l_1	11.5	w_1	11.65
W_p	24.5	l_2	9.6	w_2	9.75
t_1	1.5	l_3	7.7	w_3	7.85
t_2	0.4	l_4	5.8	w_4	5.95

Table 4. The calculated effective current path L_e and the corresponding guided wavelength for each resonance frequency f_r.

Parameter	Value (mm)	Parameter	Value (mm)
$L_{0.9\,\mathrm{GHz}}$	51.02	$0.25\lambda_{0.9\,\mathrm{GHz}}$	51.20
$L_{2.4\,\mathrm{GHz}}$	21.25	$0.25\lambda_{2.4\,\mathrm{GHz}}$	19.20
$L_{3.55\,\mathrm{GHz}}$	25.95	$0.5\lambda_{3.55\,\mathrm{GHz}}$	24.50
$L_{5.8\,\mathrm{GHz}}$	7.77	$0.25\lambda_{5.8\,\mathrm{GHz}}$	7.94

3.7.2. Realized Gain and Efficiency

Figure 17 depicts the realized gain and efficiency at the operating frequency bands for the proposed antenna. Figure 17(a) of this figure clarifies that more gain is obtained at higher frequency bands, bands 2–4 (1.17, 1.45, and 1.96 dB for 2.4, 3.5, and 5.8 GHz, respectively) compared with gain at the lower band, band 1 (−11.33 dB at 0.9 GHz). On the other hand, Figure 17(b) indicates that antenna efficiencies at the specified frequency in the aforementioned four bands are 27.04, 83.06, 75.61, and 59.11%, respectively. As stated earlier, Figure 17 demonstrates that more gain and efficiency can be obtained at higher frequency band than at lower frequency band.

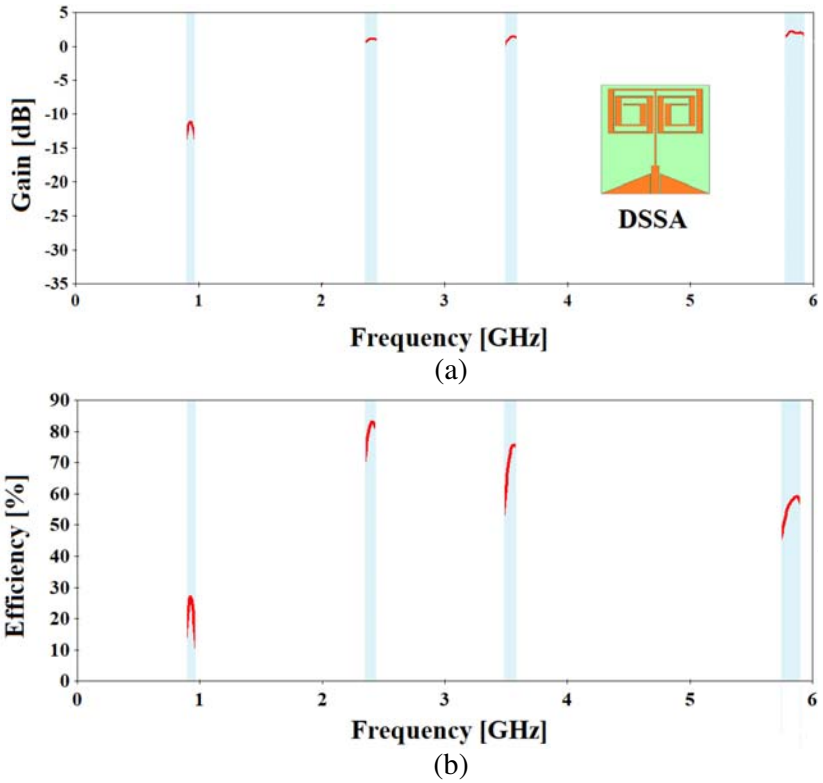

Figure 17. Simulated realized gain (a) and total efficiency (b) for the proposed antenna.

3.7.3. Radiation Patterns

Both the 3D and 2D radiation patterns for the proposed antenna at the resonance frequency in each of the four operating frequency bands (0.9 GHz, 2.4 GHz, 3.5 GHz, and 5.8 GHz) are investigated in this section. Figure 18 plots the 3D patterns at the aforementioned frequencies. It can be seen from this figure that the antenna has omnidirectional characteristic in the first three lower frequencies whereas it

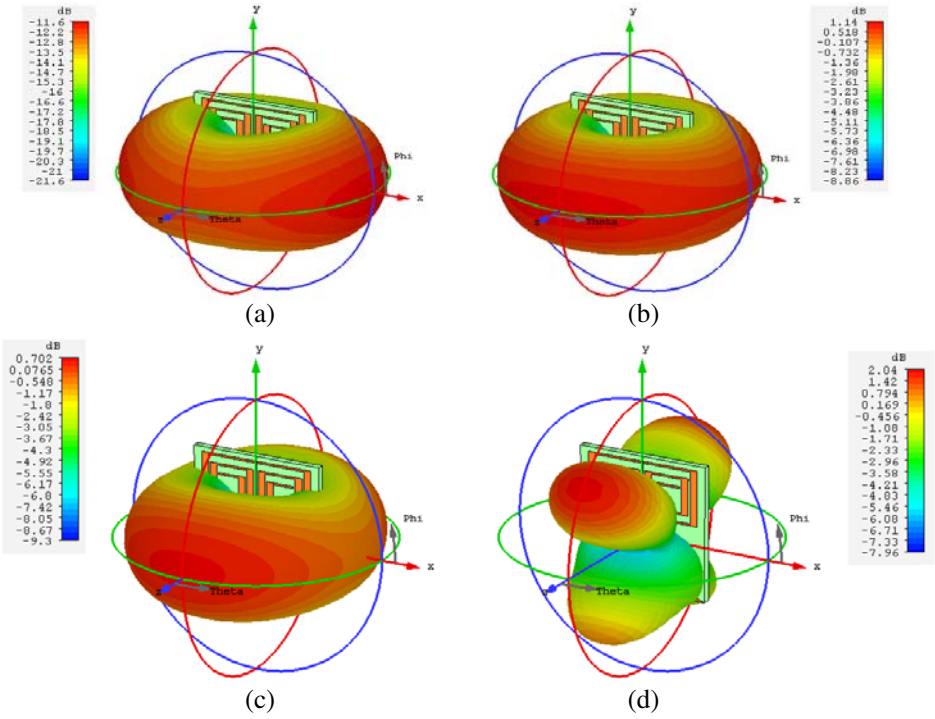

Figure 18. 3D Radiation patterns of the proposed antenna at (a) 0.9 GHz, (b) 2.4 GHz, (c) 3.5 GHz and (d) 5.8 GHz.

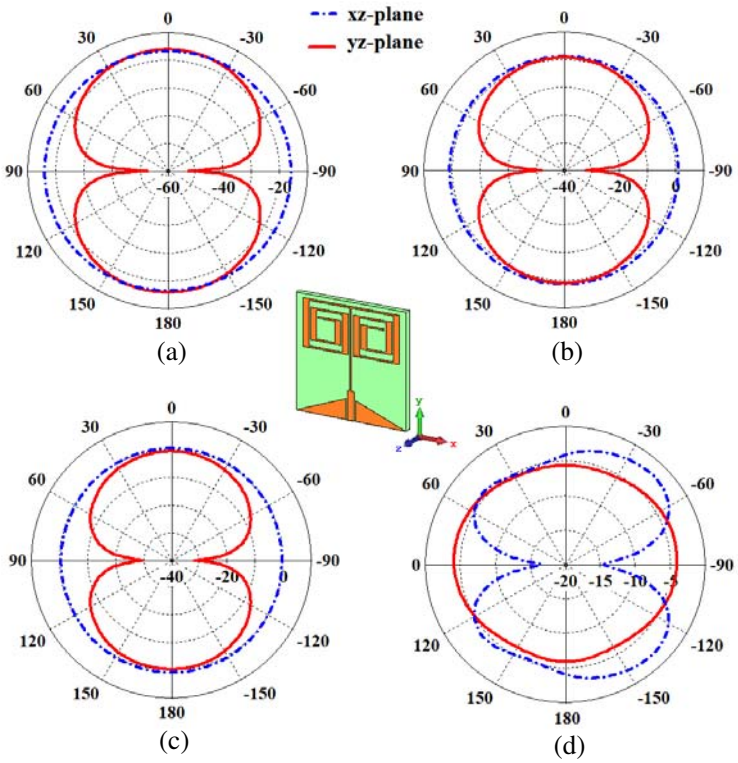

Figure 19. 2D radiation patterns of optimized antenna at (a) 0.9 GHz, (b) 2.4 GHz, (c) 3.5 GHz and (d) 5.8 GHz.

Table 5. A comparison between recent published multiband antennas and the proposed antenna in this work.

[Ref]	Antenna type	Physical size, $L_{sub} \times W_{sub}$, (mm^2)	Electrical size, $L_{sub} \times W_{sub}$, [λ_0^2]	Operating band, or centre frequency [GHz]	Realized gain [dB], Efficiency [%]
[5]	CPW-fed: Monopole + 3 resonators	35 × 32 1120 mm^2	0.2667 × 0.2917, 0.0778λ_0^2	2.50 – 2.70 3.20 – 3.55 4.95 – 5.53 5.65 – 7.20	0 dB, 87% 1.6 dB, 87% 1.2 dB, 71% -2.1 dB, 85%
[6]	CPW-fed: Monopole + metamaterial + ground + via pin	12 × 50, 600 mm^2	0.1533 × 0.0386, 0.0056 λ_0^2	0.92 2.89	-0.92 dB, 41.1% 2.59 dB, 97.5%
[12]	Stripline-fed: Triangle + slot	64.8 × 80.8 5235 mm^2	0.2262 × 0.1814, 0.0410λ_0^2	0.840 – 1.004 2.234 – 2.934	NA%, NA% NA%, NA% NA%, NA%
[13]	CPW-fed: Monopole + U-, F- and L-shaped slot	30 × 30 900 mm^2	0.0945 × 0.0945, 0.0089λ_0^2	0.945 2.500 3.520 5.800	-3.750 dBi, NA% -2.790 dBi, NA% 9.570 dBi, NA% 9.190 dBi, NA%
[14]	CPW-fed: Monopole + Spiral strip	40 × 32 1280 mm^2	0.0768 × 0.096, 0.0074λ_0^2	0.720 3.100 5.580	-13 dB, 78% 9 dB, 85% -10 dB, 87%
[15]	CPW-fed: Monopole + circular disc	105 × 175 18375 mm^2	0.4317 × 0.2590, 0.1118λ_0^2	0.74 2.45 3.50 5.80	1.3 dB, NA% 4.0 dB, NA% 6.5 dB, NA% 7.2 dB, NA%
[16]	Stripline-fed: Fractal + slot	69.6 × 72.0 5011 mm^2	0.2196 × 0.2123, 0.0466λ_0^2	0.915 2.45 5.8	3.25 dB, NA% 2.62 dB, NA% 3.31 dB, NA%
[17]	ACPW-fed: Monopole + metamaterial	40 × 24 960 mm^2	0.1232 × 0.2053, 0.0253λ_0^2	1.54 – 1.62 2.37 – 2.76 3.11 – 3.73 5.06 – 6.15	0.30 dB, 70% 2.50 dB, 82% 2.65 dB, 83% 2.60 dB, 85%
This work	CPW-fed: Monopole + Spiral strip +	28 × 28 784 mm^2	0.078 × 0.078, 0.0053λ_0^2	0.872 – 0.929 2.394 – 2.510 3.474 – 3.547 5.697 – 5.903	-11.33, 27.04% 1.17, 83.06% 1.45, 75.61% 1.96, 59.11%

radiates in many different directions at the higher frequency band. Figure 19 displays the 2D radiation patterns in the xz- and yz-planes at each of the four operating bands. It is clear from this figure that the proposed antenna has an omnidirectional radiation in xz-plane and a bidirectional radiation in yz-plane over the first three resonant frequencies, whereas the antenna has nearly omnidirectional radiation at yz-plane and a distorted figure of eight in the xz-plane.

4. COMPARISON WITH ANTENNAS REPORTED IN THE PREVIOUS LITERATURE

Table 5 presents a performance comparison between the optimized antenna presented in this work and some multiband antennas published in recent references. It is clear from this comparison that the proposed antenna has a total area of just 748 mm^2 or $0.0053\lambda_0^2$, where λ_0 is the free space wavelength at the first lower frequency, which is the smallest area compared with all published areas of the antennas listed in this table. However, as noticed from Table 5, there are a few disadvantages or drawbacks related to designing the antenna present in this work. As mentioned before, the antenna is highly miniaturized and thus offers lower gain and efficiency than previous antennas.

5. CONCLUSION

A new miniaturized multiband antenna has been introduced in this paper. The proposed antenna has overall dimensions of 28 mm $\times$ 28 mm, and it is based on a dual-arm spiral strip as radiating element and a tapered CPW-fed structure to excite this antenna. A new design approach has been presented for designing the proposed antenna for effectively operating within four frequency bands suitable for 915-MHz RFID band, 3.5-GHz WiMAX band, and the two ISM bands, 2.45 and 5.8 GHz. A CST MWS has been used to design the prototype antenna structure. Its S_{11} simulated results are compared with the experimental ones, and a good agreement between them has been obtained. Based on the experimental results, quad-band frequency range can be provided from the designed antenna, 900-MHz (872–929 MHz), 2.45-GHz (2395–2510 MHz), 3.5-GHz (3470–3550 MHz), and 5.8-GHz (5698–5900 MHz) which are compatible with the RFID, WLAN, and WiMAX applications. Furthermore, omnidirectional radiation patterns with somewhat satisfactory gains and efficiencies make it an appropriate candidate as an internal antenna for multiband wireless communication systems.

ACKNOWLEDGMENT

The authors would like to acknowledge Dr. Ghassan N. Jawad from the University of Baghdad for providing the measurement results.

REFERENCES

1. Wang, R., L.-J. Zhang, and S.-W. Hu, "A novel ACPW-fed quad-band hybrid antenna for wireless applications," *International Journal of Microwave and Wireless Technologies*, Vol. 10, No. 4, 460–468, May 2018.
2. Liu, H.-W., P. Wen, S.-S. Zhu, B.-P. Ren, X.-H. Guan, and H. Yu, "Quad-band CPW-fed monopole antenna based on flexible pentangle-loop radiator," *IEEE Antennas Wireless Propag. Lett.*, Vol. 14, 1373–1376, 2015.
3. Du, Y. Y. and A. P. Zhao, "An internal quad-band printed monopole antenna for oval-shaped mobile terminals," *IEEE Trans. Magn.*, Vol. 48, 683–686, 2012.
4. Chen, C.-C., C.-Y.-D. Sim, and F.-S. Chen, "A novel compact quad-band narrow strip-loaded printed monopole antenna," *IEEE Antennas Wireless Propag. Lett.*, Vol. 8, 974–976, 2009.
5. Abdalla, M. A. and Z. Hu, "Design and analysis of a compact quad band loaded monopole antenna with independent resonators," *International Journal of Microwave and Wireless Technologies*, Vol. 10, No. 4, 479–486, 2018.

6. Boukarkar, A., X.-Q. Lin, Y. Jiang, and Y.-Q. Yu, "Miniaturized single feed multiband patch antennas," *IEEE Trans. Antennas Propag.*, Vol. 65, 850–854, 2017.
7. Dabas, T., B. K. Kanaujia, D. Gangwar, A. K. Gautam, and K. Rambabu, "Design of multiband multipolarised single feed patch antenna," *IET Microw. Antennas Propag.*, Vol. 12, No. 15, 2372–2378, 2018.
8. Alam, M. J., M. R. I. Faruque, M. M. Hasan, and M. T. Islam, "Split quadrilateral miniaturised multiband microstrip patch antenna design for modern communication system," *IET Microw. Antennas Propag.*, Vol. 11, No. 9, 1317–1323, 2017.
9. Cao, Y.-F., S.-W. Cheung, and T.-I. Yuk, "A multiband slot antenna for GPS/WiMAX/WLAN systems," *IEEE Trans. Antennas Propag.*, Vol. 63, 952–958, 2015.
10. Mandal, D. and S. S. Pattnaik, "Quad-band wearable slot antenna with Low SAR values for 1.8 GHz DCS, 2.4 GHz WLAN and 3.6/5.5 GHz WiMAX Applications," *Progress In Electromagnetics Research B*, Vol. 81, 163–182, 2018.
11. Gautam, A. K., L. Kumar, B. K. Kanaujia, and K. Rambabu, "Design of compact F-shaped slot triple-band antenna for WLAN/WiMAX applications," *IEEE Trans. Antennas Propag.*, Vol. 64, No. 3, 1101–1105, 2016.
12. Dehmas, M., A. Azrar, F. Mouhouche, K. Djafri, and M. Challal, "Compact dual band slotted triangular monopole antenna for RFID applications," *Microw Opt. Technol. Lett.*, Vol. 60, 432–436, 2018.
13. Li, H., Y. Zhou, X. Mou, Z. Ji, H. Yu, and L. Wang, "Miniature four-band CPW-fed antenna for RFID/WiMAX/WLAN applications," *IEEE Antennas Wireless Propag. Lett.*, Vol. 13, 2014.
14. Ghosh, S. K. and R. K. Badhai, "Spiral shaped multi frequency printed antenna for mobile wireless and biomedical applications," *Wireless Pers. Commun.*, October 2017.
15. Łukasz, J., P. D. Barba, J. Łukasz, and H. Sławomir, "Many-objective automated optimization of a four-band antenna for multiband wireless sensor networks," *Sensors*, 18, 2018.
16. Mohamed, I., A. Elhassane, B. Hamid, H. Mostafa, and L. Mohamed, "Design of compact tri-band fractal antenna for RFID readers," *International Journal of Electrical and Computer Engineering (IJECE)*, Vol. 7, No. 4, 2036–2044, August 2017.
17. Sharma, S. K., M. A. Abdalla, and Z. Hu, "Miniaturisation of an electrically small metamaterial inspired antenna using additional conducting layer," *IET Microw. Antennas Propag*, Vol. 12, No. 8, 1444–1449, 2018.
18. Balanis, C. A., *Antenna Theory Analysis and Design*, 4th edition, John Wiley & Sons, 2016.